

A Novel Model on Phase Noise of Ring Oscillator Based on Last Passage Time

Bosco H. Leung, *Senior Member, IEEE*

Abstract—Ring oscillators' phase noise, when their delay cells are modeled as buffers and the noise sources assumed to be thermal noise, has some distinctive characteristics. We investigate one of the distinct characteristics, the threshold crossing property. The resulting model is shown to arise from the last passage time behavior of thermal noise present in the circuits. Simulation results on ring oscillators operating in gigahertz range and having timing jitter in picoseconds range confirm the model.

Index Terms—Jitter, phase noise, ring oscillator.

I. INTRODUCTION

PRECISE timing information required in many applications has increased the demand for low-noise clocks or oscillators. The noise present in the active and passive devices which make up these circuits modifies the phase of the oscillator output waveform in a random fashion, called timing error or phase noise. This timing error often sets the performance limit on systems in which such clocks and oscillators are being used, which range from communication receivers, disk drive systems, local area networks and microprocessors.

Previously, *LC*-based oscillators were widely used in the above applications and papers were published that predict noise in these oscillators [1], [2]. More recently, ring oscillators were also used in such applications. In contrast to *LC*-based oscillators, ring oscillators do not require inductor and can be easily fabricated in integrated form.

Past studies of timing errors in ring oscillators [3]–[7], [9] were more from a circuit viewpoint where the oscillator was treated as a time varying circuit. Inherent nonlinearity in the oscillator poses great challenge toward finding a complete solution. This paper attempts to complement these past studies by studying the noise process from a combination of circuit and probability viewpoints (using the concept of Brownian motion (Wiener process)). Specifically, the phase noise due to the distinct characteristics of threshold crossing is studied.

Section II gives a broad overview of the ring oscillator and defines the timing error used in this paper. Section III highlights the inadequacy of traditional first passage time (FPT) model and explains the need for the last passage time (LPT) model in representing the threshold crossing behavior. It then goes into detail development of this model. Section IV then derives the timing jitter based on the LPT model. Next, Section V gives

numerical examples and design curves based on the new LPT model and conclusions are drawn in Section VI.

II. RING OSCILLATOR AND MODEL

A popular N -stage ring oscillator is one based on N delay cells or stages, typically realized using N inverters, as shown in Fig. 1. For single ended inverter N is an odd number.

Some typical delay cells were analyzed in [6], [9]. An example of a delay cell, which is similar to the one discussed in [6] is shown in Fig. 2 where noise sources are explicitly shown. For this paper we limit our scope to concentrate on thermal noise only and will not address flicker noise. For this delay cell M_3 , M_4 are nominally biased to operate in saturation, and therefore behave like current sources. In this paper, the delay cell is assumed to operate in a saturated mode [5], [6], [10], which means the switching transistors completely turn on/off.

To analyze the noise behavior in more detail let us take noise sources in Fig. 2 lump them together and calculate their effects on the crossing time of the individual delay cells.

Shown in Fig. 3 is the output waveform V_{out}^+ of delay cells with noise injected, where b is the barrier. The noise in the ramp makes the ramp cross the threshold voltage with uncertainty. This uncertainty is described by t_{single} , the single-stage error. This single-stage error accumulates to form cycle-to-cycle error, t_{cycle} . Its standard deviation, the cycle-to-cycle jitter, Δt_{cycle} , is defined as the jitter per cycle of oscillation [3]–[5]. We next assume typically the ring oscillator operates inside a phase locked loop/delay locked loop (PLL/DLL). As shown in [3]–[5], when locked in a PLL/DLL, the accumulated phase error of a ring oscillator relative to a fixed reference transition, t_{acc} , does not grow indefinitely. The total rms. jitter, Δt_{acc} , which is the standard deviation of t_{acc} , is α times Δt_{cycle} , where α is independent of the ring oscillator design (only depends on PLL bandwidth). We therefore follow [3]–[5] and use Δt_{cycle} to characterize the ring oscillator timing jitter.

III. TIMING JITTER MODEL

A. Review of Ideal Buffer Model and the Resulting FPT Model

Let us review the timing jitter model for a saturated ring oscillator using the ideal buffer model [6]. For illustration purposes, we use the single-ended representation of the differential pair shown in Fig. 2 and assume the switching threshold $V_{threshold}$ is at $V_{dd} - V_{swing}/2$, where V_{swing} is voltage swing. Finally, we are interested in modeling the circuit primarily around the instant when the ramp crosses $V_{threshold}$. The resulting model is shown in Fig. 4.

Manuscript received June 26, 2002; revised September 18, 2003. This paper was recommended by Associate Editor A. Hajimiri.

The author is with the Electrical and Computer Engineering Department, University of Waterloo, Waterloo, ON N2L 3G1, Canada (e-mail: leung@vlsi.uwaterloo.ca).

Digital Object Identifier 10.1109/TCSI.2004.823658

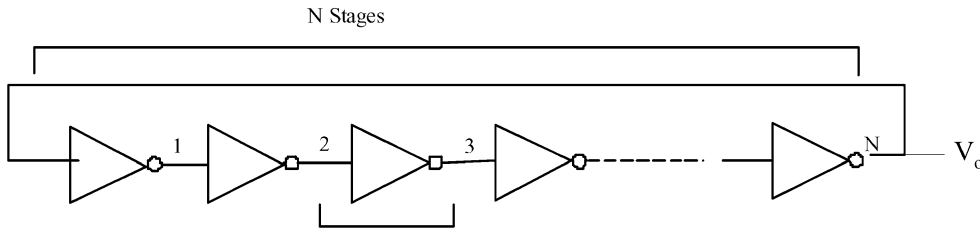


Fig. 1. Block diagram of ring oscillator.

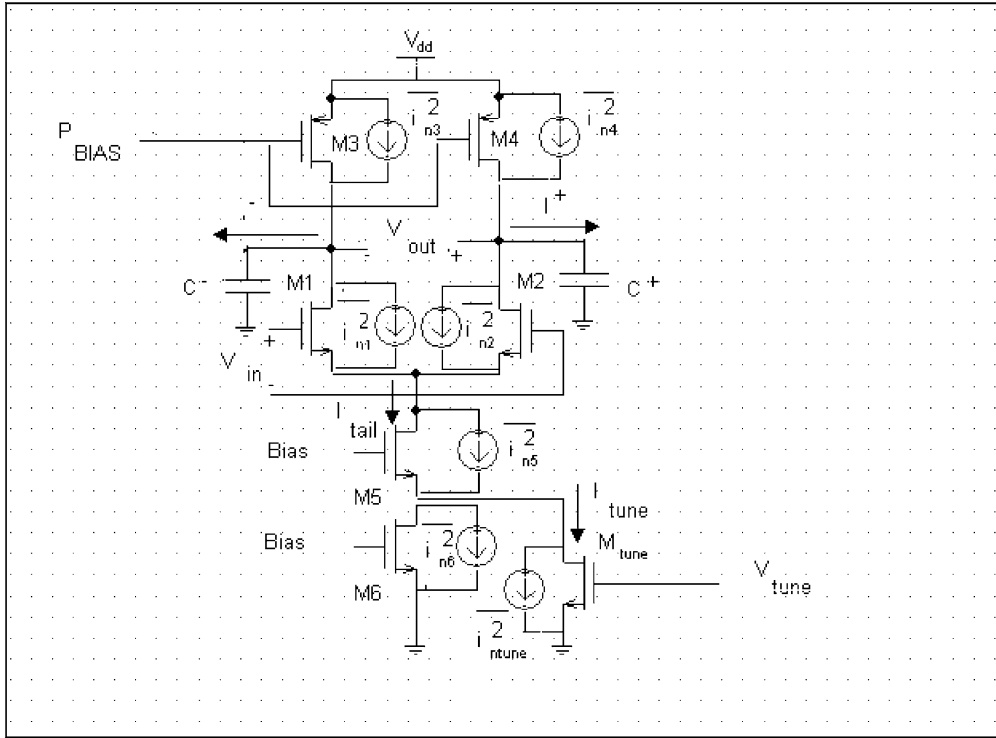


Fig. 2. Saturated delay cell, with noise sources explicitly shown.

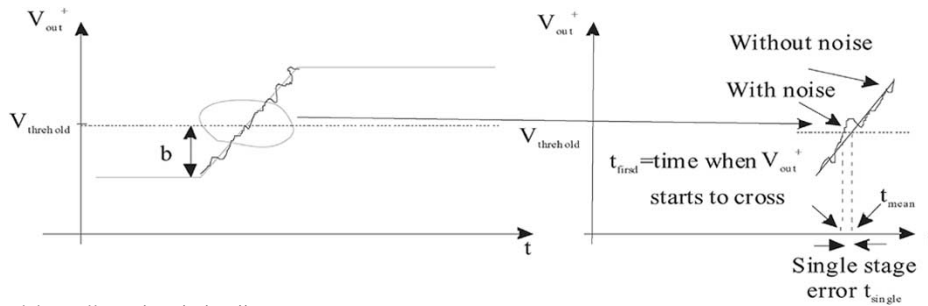


Fig. 3. Noise induced in delay cell causing timing jitter.

Using the block-labeled delay cell as an example, we shall explain how the switches function. In the delay cell, the switch SW0 is controlled by the inverter output voltage V_{o1} . If V_{o1} is high, SW0 connects node1 to the upper current source, which charges up C_0 . V_{in2} ramps up toward V_{dd} as shown in Fig. 5(a). According to the ideal buffer model, when V_{in2} goes above the threshold at t_1 , V_{o2} changes to a low state. This makes the switch SW1 connect node2 to the lower current source. V_{in3} now ramps down toward 0. Meanwhile V_{in2} keeps ramping toward V_{dd} . The upper current source has current value I , which includes all the noise sources shown in Fig. 2 and is represented as

$$I = I_{det} + I_n. \quad (1)$$

I_{det} is a deterministic current. I_n comes from thermal noise.

Conversely, if V_{o1} is low, SW0 connects node1 to the lower current source and exactly the opposite to what happened previously now occurs. Switches SW1, SW2 operate in a similar fashion.

In addition, the ideal buffer model further assumes that the maximum value V_{in2} can reach is V_{dd} , that effects such as the amplification and filtering of noise in one delay cell by the following delay cell is not included, that noise in the delay cells is uncorrelated for cycle to cycle, and that the random time $t_4 - t_1$ is independent of the random time t_1 . Finally, from symmetry, $t_4 - t_1$ and t_1 are assumed to have identical distributions. With these assumptions cycle-to-cycle jitter can be related to single-stage jitter as follows [3]–[5]:

$$\Delta t_{cycle} = \sqrt{(2N)} \times \Delta t_{single}. \quad (2)$$

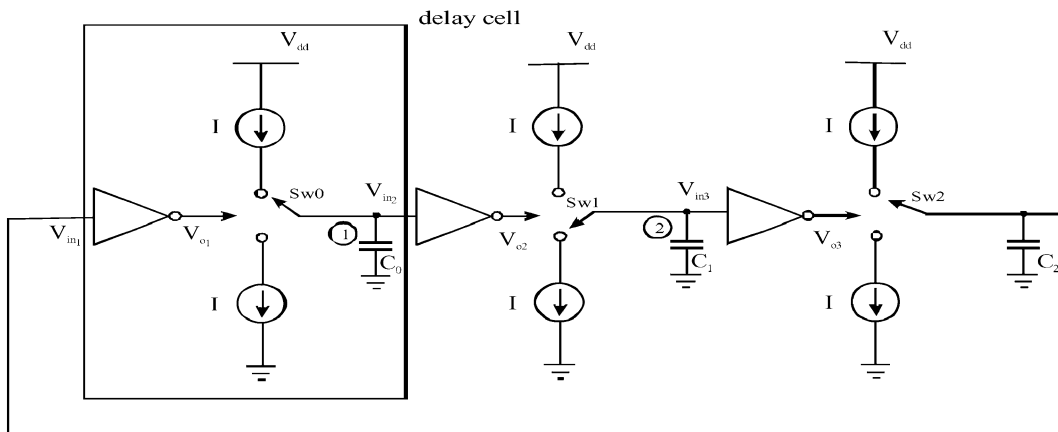


Fig. 4. Model for ring oscillator during threshold crossing.

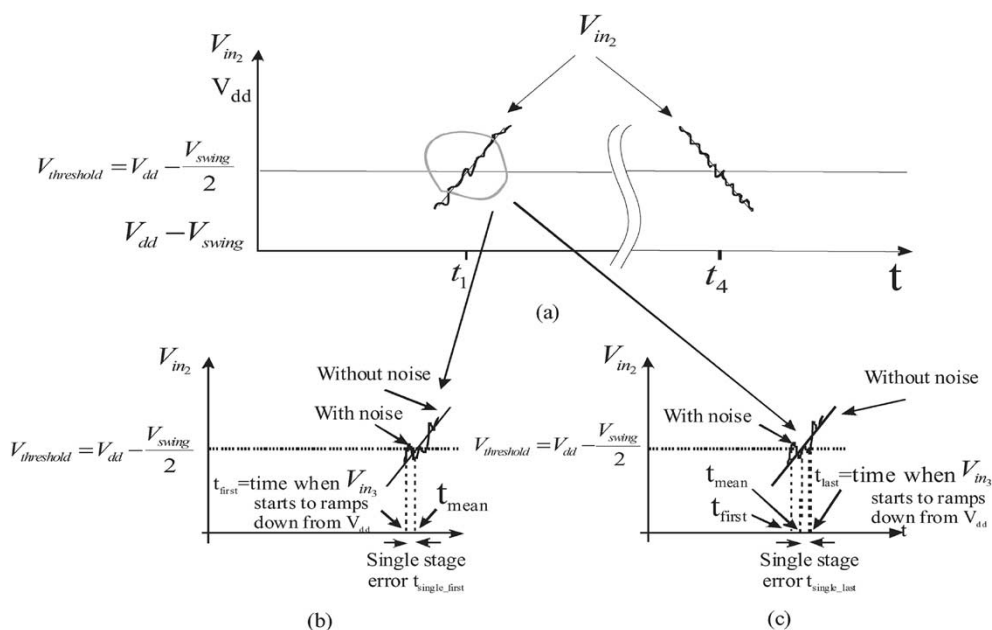


Fig. 5. Detail waveforms around threshold crossing.

TABLE I
DISTINCT CHARACTERISTICS OF MODEL ON RING OSCILLATORS

Distinct Characteristics	
1	2
Nature of threshold crossing and its impact on calculating Δt_{single} [this work]	Nature of time varying current, voltage and its impact on calculating Δt_{single} [8]

From (2), cycle-to-cycle jitter is completely characterized by single-stage jitter. Next, let us show how to find Δt_{single} .

In developing a model to calculate Δt_{single} , there are two distinct characteristics, as shown in Table I. This paper deals with the first characteristics, namely, by developing more accurate model for threshold crossing and solving the resulting Δt_{single} in a form which gives design insight. Another work by this author [8] deals with the second characteristics, namely, by developing more accurate model that accounts for the time varying current/noise around threshold and solving the resulting Δt_{single} in close form solution that yields design insights (the close form solution predicts the phase noise decreases roughly

as the *cube* of the delay cell *charging/discharging* current at the *time of threshold crossing*).

Before we develop a more accurate model for threshold crossing and solving the resulting Δt_{single} , let us review the FPT model and its formula for Δt_{single} . We focus on the part encircled in Fig. 5(a), which is expanded and shown in Fig. 5(b). In [3], [6], and [7], it was assumed that when V_{in2} crosses the threshold the first time, it triggers so that V_{in2} ramps down permanently. When this trigger mechanism is incorporated in the ideal buffer model, we have the FPT model and t_{single} that accompanies this model is denoted as $t_{\text{single_first}}$, with corresponding jitter $\Delta t_{\text{single_first}}$. Furthermore, in the special

case when I_{det} in (1) is taken as a constant current denoted as I_{dc} , $\Delta t_{\text{single_first}}$ was derived in [3] and [6] as

$$\Delta t_{\text{single_first}} = \frac{\Delta v_n}{\left(\frac{I_{\text{dc}}}{C}\right)} \quad (3)$$

where Δv_n is the standard deviation of the noise part of V_{in2} due to I_n .

B. New Last Passage Time Model

The FPT model does not model the triggering mechanism completely. Let us redraw Fig. 5(b) in Fig. 5(c) again and see what in fact is a more realistic triggering mechanism. In both Fig. 5(b) and (c) it is seen that after V_{in2} crosses $V_{\text{threshold}}$ the first time at t_{first} , it actually jumps around the threshold and makes numerous crossings. Finally, it crosses $V_{\text{threshold}}$ one last time at t_{last} and ramps toward V_{dd} . Previously we assumed that once it crosses $V_{\text{threshold}}$ the first time, V_{in3} is triggered to rise permanently. On closer examination, one can see that during the time when it jumps across the threshold, V_{o2} jumps between low and high states a couple of times, until after t_{last} , when V_{o2} permanently settles into a high state. It is therefore more realistic to assume that only at t_{last} does V_{in3} ramp down permanently. Therefore, the single-stage error should be determined by the distribution of t_{last} , rather than by t_{first} . This distribution is called the last passage time (LPT) distribution. When the above triggering mechanism is incorporated in the ideal buffer model, we call the resulting model, the ideal buffer with LPT model or simply the LPT model. The single-stage error t_{single} that accompanies this LPT model is now denoted as $t_{\text{single_last}}$, with the corresponding jitter $\Delta t_{\text{single_last}}$. Since $\Delta t_{\text{single_last}}$ is different from $\Delta t_{\text{single_first}}$, when we substitute them in (2), the corresponding cycle-to-cycle jitters $\Delta t_{\text{cycle_first}}$ and $\Delta t_{\text{cycle_last}}$ are different. Accordingly, the corresponding total rms. jitter differs as well.

Notice because an ideal buffer model is assumed, filtering of noise in one stage by the following stage is not included. Hence, the crossings distribution in one stage does not depend on the time constant of the following stage. Therefore, irrespective of the time constant, t_{single} differs between the two models.

At this point, for completeness, we want to make a few comments on the ideal buffer model on which both FPT and LPT models are based on. This ideal buffer model given in the “delay cell” in Fig. 4 represents the “delay cell” only during the time when V_{in2} crosses the threshold. The model that covers the entire oscillation period (and which reverts to the “delay cell” in Fig. 4 during the time when V_{in2} crosses the threshold) is shown in Fig. 6. We will now demonstrate that this model satisfies the fluctuation–dissipation theorem, a theorem used in some literature [14], [15] to check the validity of noise models. Starting from Fig. 2, let us concentrate on the half circuit M_1 and M_3 . For explanation purposes, let us assume the following design parameters. $V_{\text{dd}} = 3.3$ V, V_t (threshold voltage of PMOS transistor M_3) = 0.9 V, V_{swing} (voltage swing) = 1 V, $P_{\text{bias}} = 2.3$ V. Initially, let us assume that V_{in1} is low so that M_1 is off and M_3 is on and that the voltage V_{out}^+ (which is same as V_{in2} in Fig. 4) is low at $V_{\text{dd}} - V_{\text{swing}} = 2.3$ V. Furthermore, we set P_{bias} so that M_3 is designed to operate in saturation during the threshold crossing.

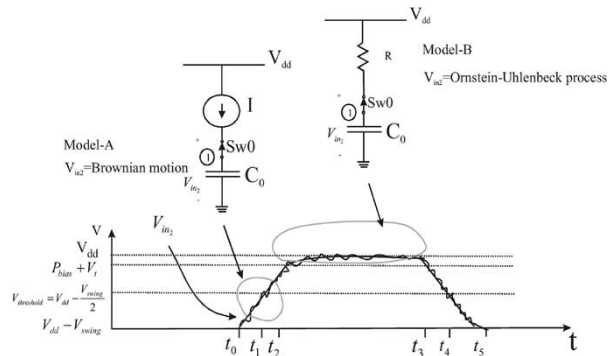


Fig. 6. Waveforms and models for the entire oscillation period.

Then, we can model M_3 as a current source which drives a capacitor. The circuit is represented by model-A in Fig. 6 and is valid from t_0 up to t_2 . During this time, V_{in2} ramps up and crosses $V_{\text{threshold}}$ (threshold voltage of the inverter M_1 and M_3 equals 2.8 V) at t_1 . If we solve the stochastic differential equation for model-A, V_{in2} is described by a Brownian motion. When V_{in2} reaches one V_t above P_{bias} (turns out to be 3.2 V) M_3 goes into triode and is modeled as a physical resistor. The circuit is now represented by model-B in Fig. 6 and is valid from t_2 to t_3 . Solving the accompanying stochastic differential, V_{in2} is now described by an Ornstein–Uhlenbeck process [14]. During this time, V_{in2} approaches V_{dd} in an exponential fashion. In summary, if we take a look at the system (transistors M_3 and M_1 , and capacitor C_0) on average (from time period t_0 to t_3), we see that there is a loss mechanism (represented by the resistor R in model-B). Therefore, the model given in Fig. 6 is consistent with the fluctuation–dissipation theorem [14], [15], which requires that the system energy be constant in an average sense. Since for passage time calculation, the result is determined mainly by the model around the instant when the ramp crosses $V_{\text{threshold}}$, that is why, in this paper, we only concentrate on the more relevant part of the whole model, model-A, in Fig. 4.

IV. DERIVATION OF SINGLE-STAGE JITTER DISTRIBUTION BASED ON LPT MODEL

A. Problem Formulation

We start from Fig. 4, which we state earlier is the “ideal buffer” model used in [6] and which has the accompanying waveform as described in Fig. 5. Fig. 5(c) is now redrawn in Fig. 7, so that the problem is described using probabilistic, rather than circuit terminology. Again, I_{det} in (1) is taken as a constant current, denoted as I_{dc} , and I_n in (1) is taken as white noise. Since the current I integrates on a capacitor to get the voltage V_{in2} , I_{dc} integrates and becomes the drift component μt and I_n integrates and become a Brownian motion σB_t . μ is the drift coefficient and σ is the variance parameter. Hence, the voltage ramp V_{in2} in Fig. 5(c) can be described as X_t , a Brownian motion with drift in Fig. 7. Accordingly, the V_{in2} ramp from $V_{\text{dd}} - V_{\text{swing}}$ to V_{dd} becomes the X_t ramp from 0 to $2b$. $V_{\text{threshold}}$ ($= V_{\text{dd}} - V_{\text{swing}}/2$) corresponds to barrier b .

Brownian motion consists of an ensemble of different paths, one of which is shown in Fig. 7. To understand the LPT problem

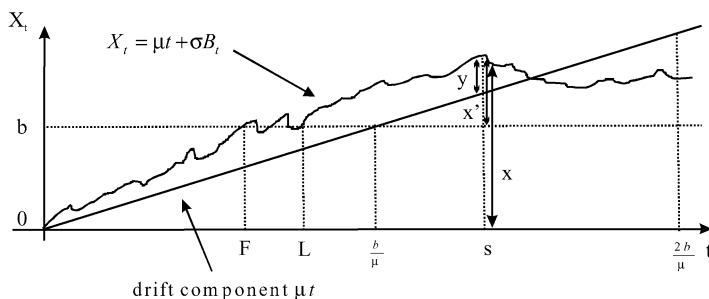


Fig. 7. Voltage ramp represented as Brownian motion with drift.

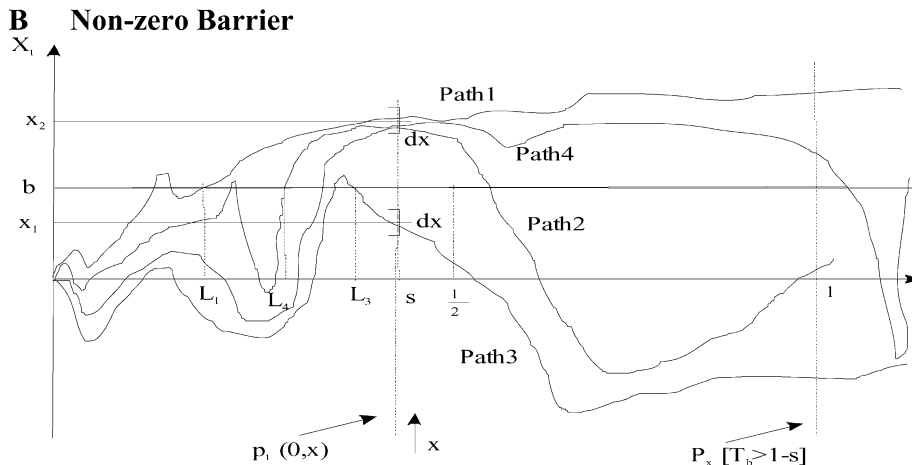


Fig. 8. Brownian motion with barrier and zero drift.

it is best to focus on the behavior of these paths. Let us see how the paths cross the barrier.

The drift component crosses at b/μ . The paths can cross before or after b/μ . Fig. 7 highlights the difference between FPT t_{first} , abbreviated here as F and LPT t_{last} , abbreviated here as L . We assume the paths must pass by a certain period less than infinity. We nominally set this to $2b/\mu$. This is because by $2b/\mu$, the drift component of X_t has reached $2b$, its maximum value. This sets the period of one delay cell nominally to $2b/\mu$, thus making the period of a N -stage ring oscillator $(2 \times N \times b)/\mu$. Next, let us define the notations we use Fig. 7.

- L LPT. This is the last time X_t crosses b from below and before $2b/\mu$.
- s Dummy variable (in time) with respect to which the cumulative distribution function (cdf) is defined.
- y How far X_t is from the drift term.
- x' How far X_t is from barrier b .
- x How far X_t is from 0.

In addition, in this paper, we use upper case for the cdf and lower case for the probability distribution function (pdf).

In the following sections, we shall find the expression for $P[L < s]$, the cdf of the LPT, by going through a series of development. The cdf will allow us to find the timing jitter. In this series of development, we start from the simplest Brownian motion and gradually build up to the Brownian motion as described in Fig. 7.

B. Nonzero Barrier

We start off with the Brownian motion (no drift) and with a barrier as described in Fig. 8. For simplicity, the period $2b/\mu$ is normalized to 1. The conclusion generalizes by extending 1 to $2b/\mu$ later on. Since there is no drift, the paths wander around with no particular direction. Their variations in Fig. 8 have been exaggerated for illustrative purposes. Our interest is to find $P(L < s)$, that is the probability of the LPT L in $[0,1]$ before a given time s . To find this probability we need to count all the paths at s that satisfies this condition. What we do is to slide (vertically) along x , at each increment “ dx ” count all the paths inside that increment, and of these paths count the one that qualifies as good path. We then sum all these good paths for x going from $-\infty$ to ∞ .

To see what qualifies as a good path, let us focus at time s . At $x = x_2$, Fig. 8 says that path1 is a good path because it passes the barrier the last time at L_1 within the time interval $[0,1]$ and L_1 is before s . To elaborate, we see path1 qualifies as a good path because:

- 1) it passes b before s (it can pass many time, the last time we call L_1);
- 2) it never passes b again before 1 (hence the pass is indeed a last pass within interval $[0,1]$).

In contrast, let us look at path2. Path2 does cross b before s , but it crosses b again after s within interval $[0,1]$ and hence does not qualify. Specifically, it fails to qualify because its LPT in $[0,1]$ is beyond s . An alternative way of expressing this failure to qualify as a good path is that looking beyond s , it passes b in the interval $[s,1]$. This is equivalent to having started from

s , its FPT upon hitting the barrier b , denoted as T_b , happens before 1. This argument can be applied in its converse form by saying that all good paths are the ones whose T_b , starting from s , happens after 1. As a check, path1, which we already argue is a good path, satisfies this argument since its T_b , starting from s , is certainly beyond 1 (from the figure path1 does not cross b again, that is its T_b can be at ∞). As another check, path 4 is also a good path, because it crosses b before s (at L_4) but does not cross b again until beyond 1. Hence, its LPT in the interval $[0,1]$ is L_4 , and as we just argue L_4 is before s . In other words, we should only count those paths which have $T_b > 1 - s$. We express the probability of the event that comprised of all these good paths as

$$\text{probability of good paths at } x = P_x[T_b > 1 - s]. \quad (4)$$

On closer look, this event is the same as the event of a typical first passage event, except the barrier changes from b to $x - b$. Since the barrier depends on x , the probability of crossing it also depends on x . We encapsulate this by putting the subscript “ x ” in P_x in (4). Obviously, the farther x is above b the less likely it is to cross the barrier, or return below b (before time 1). Conversely, this means it is more likely to cross the barrier, or return below b after time 1. In summary, we have found a way of formulating the LPT problem in terms of the FPT problem.

Let us slide along x to x_1 and look at path3. It is also a good path because it passes b before s and does not passes b in the interval $[s,1]$.

Next, we need to find out how to find the total number of paths within each increment, that is, the density of paths. This density depends on x because the density of paths of a Brownian motion spread out as we slide along x . For Brownian motion, this density has a Gaussian (or normal) distribution that centers at mean 0. This density also depends on s because for a Brownian motion its variance increases as a function of time. Finally, the density depends on where we start the Brownian motion. In this case, we start the Brownian motion at the origin. We encapsulate these dependencies on x , s and the initial starting point by writing the pdf in an increment “ dx ” at x as

$$\text{density of paths at } x = p_s(0, x). \quad (5)$$

Hence, the density of the good paths at x within a “ dx ” increment is simply the product of (4) and (5)

$$\text{density of good paths at } x = p_s(0, x) \times P_x[T_b > 1 - s]. \quad (6)$$

With this in mind, the probability of all the good paths as we slide along x is given by integrating this product through x and is

$$P[L \leq s] = \int_{-\infty}^{\infty} p_s(0, x) P_x[T_b \geq 1 - s] dx. \quad (7)$$

As a side note, let us clarify that the above probability expression includes the event path3, which crosses the barrier in the downward direction. Comparing with Fig. 7, this is not what we want. We only want the path to cross in the upward direction because we want the inverter following the block-labeled delay

cell in Fig. 4 to switch. Hence, (7) gives us the last exit time (which counts both upwards and downwards paths). We will modify this later on to count only the upward direction paths and find the probability of the event that we really want (LPT).

For the time being, let us continue on developing (7). Since we do not really know $P_x[T_b > 1 - s]$, we will now make use of a property called Markov property [16] and relate $P_x[T_b > 1 - s]$ to $P_0[T_{x-b} > 1 - s]$, something that we know. Specifically

$$P_x[T_b \geq 1 - s] = P_0[T_{x-b} \geq 1 - s]. \quad (8)$$

Substituting (8) into (7) we have

$$P[L \leq s] = \int_{-\infty}^{\infty} p_s(0, x) P_0[T_{x-b} \geq 1 - s] dx. \quad (9)$$

C. Nonzero Barrier and Drift

Let us now start to apply drift to the Brownian motion, which is shown in Fig. 9, where the drift direction is explicitly shown. The drift coefficient is μ . Again, the paths’ variations have been exaggerated for illustrative purposes. Comparing to Fig. 8, it is obvious that with drift, the Brownian motion moves upwards on “average” and crosses b earlier. As in Fig. 8, paths 1, 4 are good paths and path 2 is not, for the same reasons. Again, as in Fig. 8, path3 is a good path but since it crosses b in the downward direction, counting it gives us the last exit time, not the LPT.

How does adding drift affect the above equations? When drift μ is applied, the mean of the Brownian motion is shifted. What would it be at s , our time of interest? From Fig. 7, the drift component has a value $s\mu$ at s . This would shift the mean of the distribution by $s\mu$ and (5) becomes

$$\text{density of paths at } x = p_s(s\mu, x). \quad (10)$$

From [16], this is given as

$$p_s(s\mu, x) = \frac{1}{\sqrt{2\pi s}} e^{[-(x-s\mu)^2/2s]}. \quad (11)$$

Similarly, the distribution as given in (4) would also have its mean shifted and so (4) needs to be modified. In addition the distribution in (4) is calculated as the FPT upon hitting the barrier b under *drift*, starting at s , that happens before 1. We give it a new symbol Q_x^μ and (4) becomes

$$\text{probability of good paths at } x = Q_x^\mu[T_b > 1 - s]. \quad (12)$$

Substituting (10) and (11) into (7) we have

$$P[L \leq s] = \int_{-\infty}^{\infty} p_s(s\mu, x) Q_x^\mu[T_b \geq 1 - s] dx. \quad (13)$$

Again, using the Markov property as we have done in (8), we have

$$Q_x^\mu[T_b \geq 1 - s] = Q_0^\mu[T_{x-b} \geq 1 - s]. \quad (14)$$

To calculate $Q_0^\mu[T_b > 1 - s]$, we start from the FPT probability distribution with barrier b and a positive drift component as given in [17] where we have

$$p_0^\mu[T_b \in dt] = \frac{|b|}{\sqrt{2\pi t^3}} e^{[-(b-\mu t)^2]/2t} dt. \quad (15)$$

Our present barrier height is $x - b$. What about the sign of our drift? Referring to Fig. 9, if at s the path is already above b (like path1), as far as the barrier is concerned the path is drifting in the *negative* direction, that is the barrier is on the opposite side of where the path is drifting. On the other hand, if at s the path is below b (like path3), as far as the barrier is concerned the path is drifting in the *positive* direction. Hence, (15) has two possible expressions corresponding to two possible signs of drift

$$p_0^\mu[T_{x-b} \in dt] = \frac{|x-b|}{\sqrt{2\pi t^3}} e^{[-(x-b+\mu t)^2]/2t} dt$$

or

$$p_0^\mu[T_{x-b} \in dt] = \frac{|x-b|}{\sqrt{2\pi t^3}} e^{[-(x-b-\mu t)^2]/2t} dt. \quad (16)$$

The cdf is then given by integrating this pdf

$$\begin{aligned} Q_0^\mu[T_{x-b} \geq 1-s] &= \int_{1-s}^{\infty} p_0^\mu[T_{x-b} \in dt] dt \\ &= \int_{1-s}^{\infty} \frac{|x-b|}{\sqrt{2\pi t^3}} e^{[-(x-b+\mu t)^2]/2t} dt \\ &\quad + \int_{1-s}^{\infty} \frac{|x-b|}{\sqrt{2\pi t^3}} e^{[-(x-b-\mu t)^2]/2t} dt. \end{aligned} \quad (17)$$

Substituting (11) and (17) into (13), we have (18) shown at the bottom of the page.

D. Nonzero Barrier and Drift With Upward Counting Only

Let us go back to Fig. 8 and examine path3. In Sections IV-B and IV-C, we briefly mention that path3 qualifies as good path under the “last exit time” principle but not under the “LPT” principle. We shall clarify this further in this section.

By the “last exit time” we mean the path only needs to cross the boundary b the last time before s in the interval $[0,1]$. As path3 does exactly that, it qualifies. But comparing with X_t , our desired path in Fig. 7, this is definitely not a path we want. This is because path3 stays under the barrier b and the inverter following the delay cell will not have switched. So, what qualifies a *real good* path? Obviously one whose value in $[s,1]$ is above b . Furthermore since a good path cannot cross anymore in $[s,1]$, this means its *entire* value in $[s,1]$ must be above b . What does this say about its value at s ? If its value at s is below b at s , for its final value to be above b , it must cross b again, thus violating the above qualification as a good path (its LPT will be

beyond s). Consequently real good paths must have their values at s larger than or equal to b . We differentiate these two cases by calling the event that counts every good path, including path3, as “last exit time” event and the event that counts every good path, excluding path3, as “LPT” event. Obviously, the “LPT” event is a subset of “last exit time” event. To obtain the “LPT” event from the “last exit time” event we modify the integration along x from $x = -\infty$ to ∞ to $x = b$ to ∞ . Also, since only paths with value at s above b is counted, $Q_x^\mu[T_b > 1 - s]$ in (17) is evaluated with *negative* drift only. With these modifications (18) becomes

$$\int_b^{\infty} \frac{1}{\sqrt{2\pi s}} e^{[-(x-\mu s)^2]/2s} \left\{ \int_{1-s}^{\infty} \frac{|x-b|}{\sqrt{2\pi t^3}} e^{[-(x-b+\mu t)^2]/2t} dt \right\} dx. \quad (19)$$

When the integration limit is modified, the sample space is also modified. The reduced sample space contains only those paths which is above b at $s = 1$. Since we are still interested in the cdf of the LPT, we need to reflect this fact through renormalization. When we apply this renormalization to (19), we obtain the cdf of the LPT under this new sample space as

$$\begin{aligned} P[L \leq s] &= \frac{\int_b^{\infty} \frac{1}{\sqrt{2\pi s}} e^{[-(x-\mu s)^2]/2s} \left\{ \int_{1-s}^{\infty} \frac{x-b}{\sqrt{2\pi t^3}} e^{[-(x-b+\mu t)^2]/2t} dt \right\} dx}{\int_b^{\infty} \frac{1}{\sqrt{2\pi \times 1}} e^{[-(x-2b)^2]/2 \times 1} dx}. \end{aligned} \quad (20)$$

E. Complete Noise Model

Refer to Fig. 7. Let us define $x' = x - b$. Substituting this in (20) we finally have

$$\begin{aligned} P[L \leq s] &= \frac{\int_0^{\infty} \frac{1}{\sqrt{2\pi s}} e^{[-(x'+b-\mu s)^2]/2s} \left\{ \int_{1-s}^{\infty} \frac{x'}{\sqrt{2\pi t^3}} e^{[-(x'+\mu t)^2]/2t} dt \right\} dx'}{\int_0^{\infty} \frac{1}{\sqrt{2\pi \times 1}} e^{[-(x'-b)^2]/2 \times 1} dx'}. \end{aligned} \quad (21)$$

There is one more qualification one has to observe. In (17), we have separated the Q for positive and negative drifts by simply changing the sign of μ . However, for *negative* drift there is one more complication. Referring to Fig. 9 let us focus on a path that corresponds to the negative drift case, like path1. Beyond s , the path is seen to lie above the barrier while the drift still takes the path in the upward direction. Hence, it is possible that the path will never cross b again, even at $t = \infty$. In other words integrating t up to ∞ does not count all the paths. The proper expression should have been calculated by finding the probability of all the paths ($= 1$) minus the probability of the FPT in the remaining interval. The remaining interval is given by

$$\begin{aligned} P[L \leq s] &= \int_{-\infty}^{\infty} \frac{1}{\sqrt{2\pi s}} e^{[-(x-\mu s)^2]/2s} \left\{ \int_{1-s}^{\infty} \frac{|x-b|}{\sqrt{2\pi t^3}} e^{[-(x-b+\mu t)^2]/2t} dt \right\} dx \text{ or} \\ &\quad \int_{-\infty}^{\infty} \frac{1}{\sqrt{2\pi s}} e^{[-(x-\mu s)^2]/2s} \left\{ \int_{1-s}^{\infty} \frac{|x-b|}{\sqrt{2\pi t^3}} e^{[-(x-b-\mu t)^2]/2t} dt \right\} dx \end{aligned} \quad (18)$$

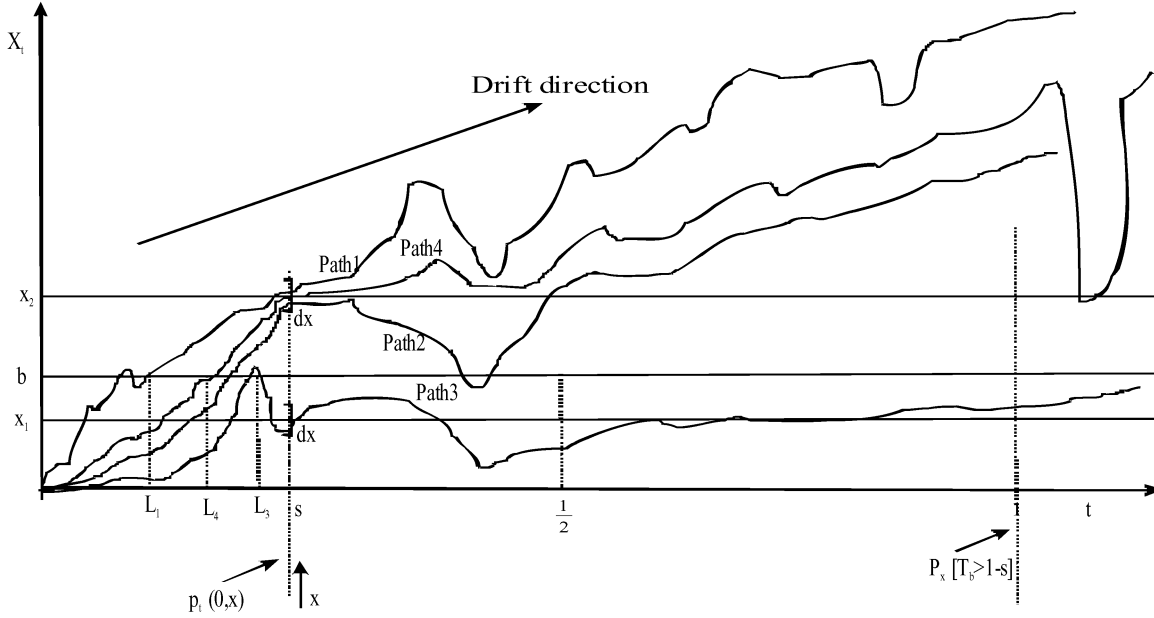


Fig. 9. Brownian motion with barrier and finite drift.

$[0, \infty] - [1 - s, \infty] = [0, 1 - s]$. The expression in (17) then becomes $1 - \int_0^{1-s} (|x - b|/\sqrt{2\pi t^3}) e^{[-(x-b-\mu t)^2/2t]} dt$. With this expression and $x' = x - b$ again, (21) becomes

$$P[L \leq s] = \frac{\int_0^\infty \frac{1}{\sqrt{2\pi s}} e^{[-(x'+b-\mu s)^2/2s]} \left\{ 1 - \int_0^{1-s} \frac{x'}{\sqrt{2\pi t^3}} e^{[-(x'-\mu t)^2/2t]} dt \right\} dx'}{\int_0^\infty \frac{1}{\sqrt{2\pi \times 1}} e^{[-(x'-b)^2/2 \times 1]} dx'} \quad (22)$$

We can now generalize the above expression to the cases where we:

- include explicit variance in the normal [13] and FPT [18] distribution;
- relax the LPT last occurrence from 1 to whatever limit we want. In Fig. 7 we have set this limit to $2b/\mu$.

Equation (22) becomes (23), shown at the bottom of the page. Equation (23) gives us the cdf of the random variable “ L ”, or t_{last} . Following the notation in [13] we write $P[L \leq s]$ as $F(s)$, since the cdf is a function of “ s ”. The corresponding pdf, again following the notation in [13], is denoted as $f(s)$. This is also a function of “ s ” and is related to $F(s)$ as

$$f(s) = \frac{dF[s]}{ds} \quad (24)$$

The mean of “ L ”, or t_{last} , is then given by

$$t_{\text{last_mean}} = E[L] = \int_0^\infty s f(s) ds \quad (25)$$

where E is the expectation operator. The single-stage jitter using LPT model, $\Delta t_{\text{single_last}}$, is the standard deviation of the random variable $t_{\text{single_last}}$. This equals the standard deviation of the random variable “ L ” and is given, following the notation in [13], as

$$\begin{aligned} \Delta t_{\text{single_last}} &= \sqrt{E[(L - t_{\text{last_mean}})^2]} \\ &= \sqrt{\int_0^\infty (s - t_{\text{last_mean}})^2 f(s) ds} \quad (26) \end{aligned}$$

V. SIMULATION RESULTS AND DESIGN GUIDELINES

In this section, we first relate the previous results developed in probability theory to terminology used in circuit design. We then go through a few numerical examples to demonstrate how to use these results to give us design guidelines.

A. Expressing LPT Expression in Terms of Circuit Design Parameters

We start from the block-labeled “delay cell” in Fig. 4 and assume we are operating in the period t_0 to t_2 in Fig. 6. During this period, SW0 connects node1 to the upper current source. The resulting circuit is shown in Fig. 10, where the voltage V_{in2} is simply labeled V . This will allow us to find the distribution of t_1 .

The circuit equation is given by

$$I = C \frac{dV}{dt} = CV' \quad (27)$$

$$P[L \leq s] = \frac{\int_0^\infty \frac{1}{\sqrt{2\pi \sigma^2 s}} e^{[-(x'+b-\mu s)^2/2\sigma^2 s]} \left\{ 1 - \int_0^{(2b/\mu)-s} \frac{x'}{\sqrt{2\pi \sigma^2 t^3}} e^{[-(x'-\mu t)^2/2\sigma^2 t]} dt \right\} dx'}{\int_0^\infty \frac{1}{\sqrt{2\pi \sigma^2 \times \frac{2b}{\mu}}} e^{[-(x'-b)^2/(2\sigma^2 \times (2b/\mu))]} dx'} \quad (23)$$

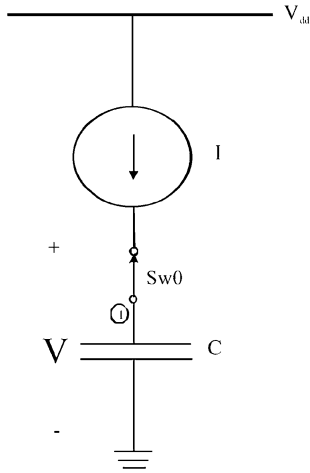


Fig. 10. Delay cell model during threshold crossing.

where the derivative (from now on) is implicitly assumed to be with respect to time t and is abbreviated by the superscript $'$. Now, from (1) we have

$$I = I_{dc} + I_n. \quad (28)$$

Here, I_n is assumed to come from thermal noise present in the current source and has a white noise characteristics. Following [12], we relate white noise to Brownian motion by treating white noise as the “derivative” of Brownian motion, as if such a derivative exists. Therefore

$$I = I_{dc} + \sigma_I B_t'. \quad (29)$$

This is a stochastic differential equation as the derivative includes a noise process [11].

Here, σ_I is the variance parameter of I_n . Substituting (29) into (27) we have

$$CV' = I_{dc} + \sigma_I B_t'. \quad (30)$$

Integrating, we have

$$CV = I_{dc}t + \int_0^t \sigma_I B_s' ds. \quad (31)$$

This can then be written as

$$CV = I_{dc}t + \int_0^t \sigma_I dB_s. \quad (32)$$

This last integral $\int_0^t \sigma_I dB_s$ is a stochastic integral. Equation (32) can now be written as

$$CV = I_{dc}t + \sigma_I B_t$$

or

$$V = \frac{I_{dc}}{C}t + \frac{\sigma_I}{C}B_t. \quad (33)$$

The advantage of writing (30) in the new form (33) is that (33) expresses the noise process in terms of Brownian motion, where the concept of passage time (first and last) can be rigorously defined. In contrast, no such concept exists for white noise. The square of the variance parameter σ_I^2 is just the value

of the psd of the thermal noise present in the current source. For the ring oscillator we are considering, we assume this current source comes from a MOS transistor biased in saturation and hence we have

$$\sigma_I^2 = 4kT \times \frac{2}{3}g_m \quad (34)$$

where g_m is its transconductance.

Returning to (33), if we compare that equation with the expression of X_t as given in Fig. 7 we find that they have the same form with

$$\mu = \frac{I_{dc}}{C} \quad (35)$$

$$\sigma = \frac{\sigma_I}{C}. \quad (36)$$

The voltage swing of the circuit gives us the barrier b .

We now have related the circuit parameters (I_{dc} , C , g_m , voltage swing) to the parameters in the LPT expression (b , μ , σ) as given in (23). This allows us to determine the distribution of t_1 . From Section III, this is also identical to the distribution t_5-t_1 in Fig. 6. Next, we will apply (26) to calculate the LPT of various designs of a ring oscillator.

B. Numerical Examples, Design Curves and Guidelines

1) *Comparisons of Cycle-to-Cycle Jitter Based on LPT/FPT Model in 0.6- μ Technology:* We want to start with the example “delay cell” given in Fig. 2 and use it to design a 4-stage 1-GHz ring oscillator. For this example, we set P_{bias} so that M_3 is designed to operate in saturation during threshold crossing. We use parameters similar to those given in [6]. There, a 0.6- μ CMOS technology with a V_{dd} of 3.3 V is adopted. Supply current per stage (I /stage) is designed to be 1.25 mA, or branch current $I_{dc} = 0.625$ mA. $V_{ds(sat)}$ is 300 mV.

With these values we have

$$g_m = \frac{I_{dc}}{(V_{GS} - V_t)} = \frac{2I_{dc}}{V_{ds(sat)}} = 4.1 \text{ m}\Omega^{-1}. \quad (37)$$

Substituting into (34), we have

$$\sigma_I = 6.9 \times 10^{-12} \frac{\text{A}}{\sqrt{\text{Hz}}}. \quad (38)$$

For a 1-GHz, 4-stage ring oscillator and a V_{swing} of 2 V (corresponding to a b of 1 V), each delay cell has

$$\mu = 8 \times 10^9 \frac{\text{V}}{\text{s}}. \quad (39)$$

Substituting this in (35) we have

$$C = 0.078 \text{ pF}. \quad (40)$$

The above σ_I is the total σ_I if we assume the noise comes from only one transistor whose g_m is given by (37). However, as shown in Fig. 2, the noise actually comes from two PMOS transistors M_3 and M_4 , the differential pair M_1 , M_2 , the current source M_5 and M_6 , as well as the tuning circuit. The total σ_I is the rms sum of the individual σ_I . These individual σ_I are normalized with respect to the σ_I of M_1 as calculated in (38). To simplify matters, we are just going to estimate the sizes of

these individual σ_I relative to that of M_1 by following similar trends as observed in [6]

$$\begin{aligned}\sigma_{I-M6} &= \sigma_{I-M_tune} = \sigma_{I-M1} \\ \sigma_{I-M3} &= \sigma_{I-M4} = \sqrt{3}\sigma_{I-M1}.\end{aligned}\quad (41)$$

With the above estimates, we have

$$\begin{aligned}\sigma_{I_total} &= \sqrt{(\sigma_{I-M3}^2 + \sigma_{I-M4}^2 + \sigma_{I-M6}^2 + \sigma_{I-M_tune}^2 \\ &\quad + \sigma_{I-M1}^2 + \sigma_{I-M2}^2)} \\ &= 2.22 \times 10^{-11} \frac{\text{A}}{\sqrt{\text{Hz}}}.\end{aligned}\quad (42)$$

Substituting this in (36) we have

$$\sigma = 284 \frac{\text{V}}{(\text{s} - \sqrt{\text{Hz}})}.\quad (43)$$

Substituting (39) and (43), into (23), we finally get the expression of the LPT cdf for the present design. Using this in (26), we can get $\Delta t_{\text{single_last}}$, which then gives us $\Delta t_{\text{cycle_last}}$, the cycle-to-cycle jitter using the LPT model. This was evaluated numerically by the software MathCad.

Because of the high degree of accuracy needed (the noise parameter of “284” is quite small compared to the drift of 8×10^9), symbolic integration (using the software Maple) is first used to get us as far to a closed-form solution as possible. Then, numerical integration is carried out. Accuracy is preserved as much as possible by carrying the full 15-digit representation allowed by the program. Whenever ∞ appears in the integration limit, the highest number allowed in the system (10^{307}) is used to represent ∞ . Numerous checks of the integration accuracy is performed, e.g., integral of the pdf over the entire sample space is checked to make sure it is 1 (to 15 digit). The following is a summary of the results. Here, $t_{\text{last_mean}}$ is the mean predicted by the LPT model. $\Delta t_{\text{cycle_first}}$ is the cycle-to-cycle jitter using the FPT model which is calculated using $\Delta t_{\text{single_first}}$ as given in (3)

$$\begin{aligned}\Delta t_{\text{cycle_first}}(8 \times 10^9, 1, 0.284 \times 10^3) &= 1.1 \text{ ps} \\ \Delta t_{\text{cycle_last}}(8 \times 10^9, 1, 0.284 \times 10^3) &= 2 \text{ ps} \\ t_{\text{last_mean}}(8 \times 10^9, 1, 0.284 \times 10^3) &= 0.5005 \text{ ns}.\end{aligned}$$

It is seen that $\Delta t_{\text{cycle_last}}$ has a value of 2 ps in a period of 1 ns (1 GHz). This is roughly -60 dBc. $\Delta t_{\text{cycle_first}}$ is calculated to be 1.1 ps. Two observations are made here. First, $\Delta t_{\text{cycle_last}}$ is larger than $\Delta t_{\text{cycle_first}}$, as expected. Secondly, the ratio $\Delta t_{\text{cycle_last}}/\Delta t_{\text{cycle_first}}$ is 1.8, indicating that the LPT model gives an answer that differs from that of the FPT model by a nonnegligible amount.

2) *Comparisons of Cycle-to-Cycle Jitter Based on LPT/FPT Model in 0.18- μ Technology:* Let us redesign the same circuit using a 0.18- μ process and operates at $V_{\text{dd}} = 2 \text{ V}$. The k' of the process is assumed to be $400 \mu\text{A}/\text{V}^2$ and C_{ox} is $7 \text{ fF}/\mu^2$. With a lower power supply, V_{swing} is scaled to 400 mV, giving a “ b ” of 200 mV. For complete switching, $V_{\text{ds(sat)}}$ is now scaled down to 50 mV. This results in the following circuit parameters $C = 0.39 \text{ pF}$, $W/L = 112 \mu/0.18 \mu$. The probability parameter becomes $\mu = 1.6 \times 10^9 \text{ 132 V/s}$, $\sigma = \text{V/s} - \sqrt{\text{Hz}}$. The

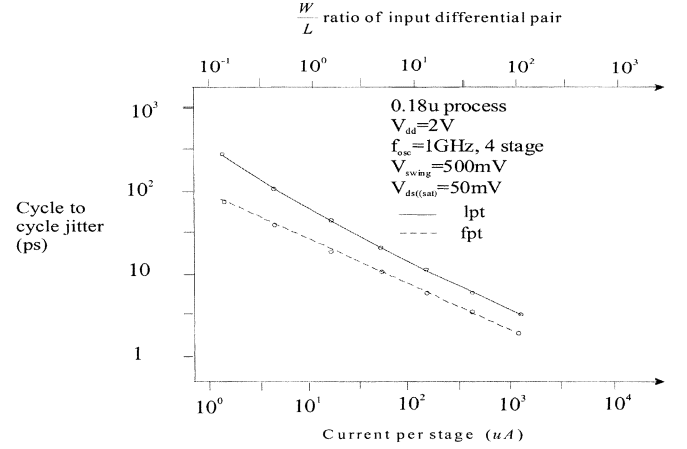


Fig. 11. Cycle-to-cycle jitter (LPT/FPT model) versus inverter size and current/stage.

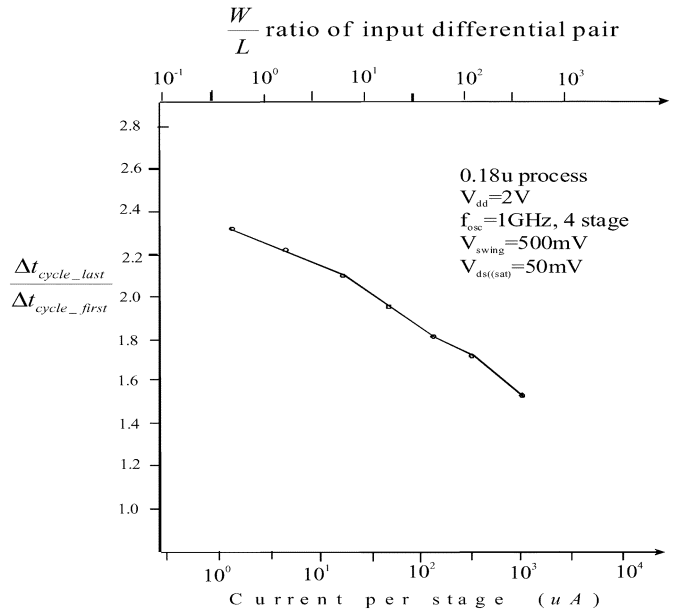


Fig. 12. Ratio of cycle-to-cycle jitter based on LPT/FPT model.

resulting $\Delta t_{\text{cycle_first}}$ and $\Delta t_{\text{cycle_last}}$ are 2.6 and 4 ps, respectively. $\Delta t_{\text{cycle_last}}/\Delta t_{\text{cycle_first}}$ is 1.5. Again, the LPT model gives an answer that differs from that of the FPT model by a nonnegligible amount.

3) *Design Curves for $\Delta t_{\text{cycle_last}}$, $\Delta t_{\text{cycle_first}}$ and $\Delta t_{\text{cycle_last}}/\Delta t_{\text{cycle_first}}$ as a Function of I/stage :* We now investigate the trend of $\Delta t_{\text{cycle_last}}$, $\Delta t_{\text{cycle_first}}$, and $\Delta t_{\text{cycle_last}}/\Delta t_{\text{cycle_first}}$ as a function of I/stage , for the same process and V_{dd} , as in case 2. As I/stage changes, I_{dc} changes. Two choices of design follow.

- 1) Fixing $V_{\text{ds(sat)}}$ and varying W/L ratio of the input differential pair.
- 2) Fixing the W/L ratio of the input differential pair and varying $V_{\text{ds(sat)}}$.

Simulations on both choices show similar dependencies for $\Delta t_{\text{cycle_last}}$, $\Delta t_{\text{cycle_first}}$, and $\Delta t_{\text{cycle_last}}/\Delta t_{\text{cycle_first}}$ on I/stage . We first show the dependencies of $\Delta t_{\text{cycle_last}}$, $\Delta t_{\text{cycle_first}}$ in in Fig. 11. We next show the dependency of $\Delta t_{\text{cycle_last}}/\Delta t_{\text{cycle_first}}$ in Fig. 12. The range of I/stage

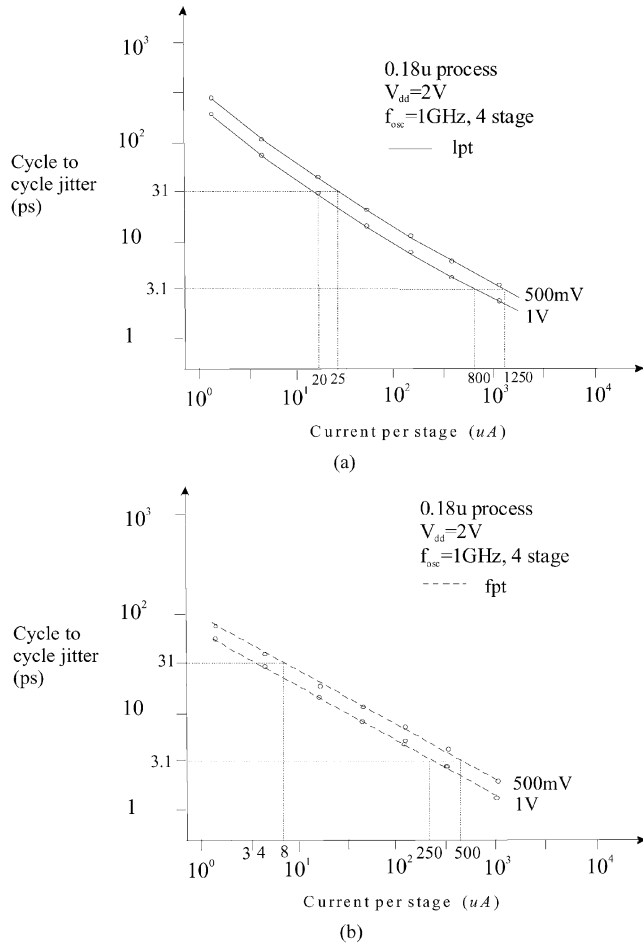


Fig. 14. Cycle-to-cycle jitter versus current/stage with voltage swing as parameter based on LPT/FPT.

in both figures is decided as follows. We start with I/stage as given in case 2 and vary it over three decades, from 1.25 mA/stage to 1.25 $\mu\text{A}/\text{stage}$. With I/stage larger than 1.25 mA, $\Delta t_{\text{cycle_last}}$ approaches $\Delta t_{\text{cycle_first}}$. With I/stage becomes smaller than 1.25 μA $\Delta t_{\text{cycle_last}}$ approaches T_{osc} , the oscillation period, in which case, we are no longer interested. The corresponding W/L ratio of the input differential pair is also given in the figures and varies from 112 u/0.18 u to 0.18 u/0.27 u. From the figures, we observe the following.

- a) $\Delta t_{\text{cycle_last}}$ is always larger than $\Delta t_{\text{cycle_first}}$ or $\Delta t_{\text{cycle_last}}/\Delta t_{\text{cycle_first}}$ is always larger than 1, as expected theoretically.
- b) As I/stage increases, $\Delta t_{\text{cycle_last}}$, $\Delta t_{\text{cycle_first}}$ both decrease. Moreover, $\Delta t_{\text{cycle_last}}/\Delta t_{\text{cycle_first}}$ decreases and approaches 1. Theoretically, as I/stage increases, phase noise decreases. Therefore, both $\Delta t_{\text{cycle_last}}$ and $\Delta t_{\text{cycle_first}}$ should decrease. Moreover, with less noise, the difference between first passage and last passage crossing is diminished and so $\Delta t_{\text{cycle_last}}/\Delta t_{\text{cycle_first}}$ should approach 1.

4) *Design Curves for $\Delta t_{\text{cycle_last}}$ as a Function of f_{osc} , V_{swing} and Some Design Guidelines:* We would now repeat case 3 with other circuit variables V_{swing} and f_{osc} , as parameters. To do this, we break the dependency of $\Delta t_{\text{cycle_last}}$

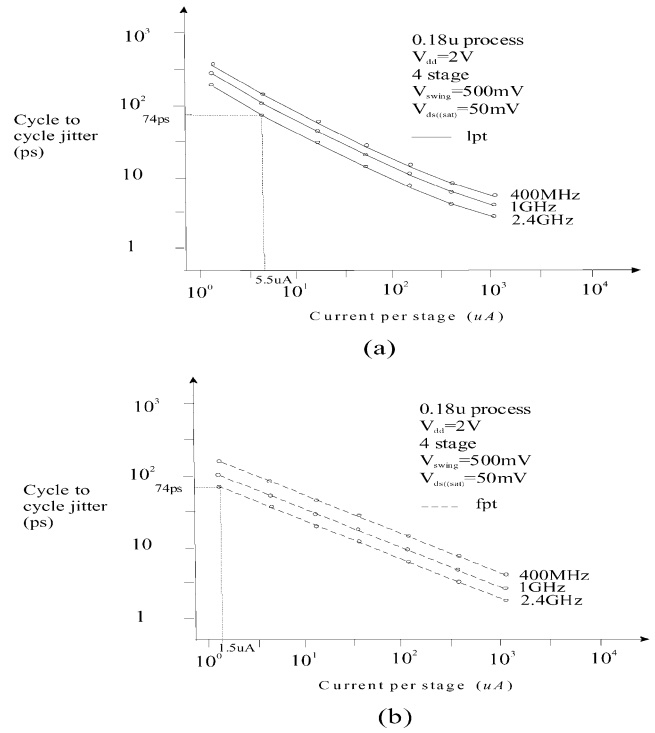


Fig. 13. Cycle-to-cycle jitter versus current/stage with oscillation frequency as parameter based on LPT/FPT.

into two separate parts, $\Delta t_{\text{cycle_last}}/\Delta t_{\text{cycle_first}}$ dependencies and $\Delta t_{\text{cycle_first}}$ dependencies. Simulations show that $\Delta t_{\text{cycle_last}}/\Delta t_{\text{cycle_first}}$ dependency on I/stage , with V_{swing} and/or f_{osc} varying, has the same general trend as shown in Fig. 12. Meanwhile, $\Delta t_{\text{cycle_first}}$ dependency on I/stage , with V_{swing} and/or f_{osc} varying, can be obtained from (3). Our approach then consists of combining Fig. 12 and (3) to find $\Delta t_{\text{cycle_last}}$ as a function of these other parameter changes. This approach is applied to the case when we repeat case 3 for $f_{\text{osc}} = 400 \text{ MHz}, 1 \text{ GHz}, \text{ and } 2.4 \text{ GHz}$. The simulation result is shown in Fig. 13(a). This approach is also applied to the case when we repeat case 3 for $V_{\text{swing}} = 500 \text{ mV}$ and 1 V. The simulation result is shown in Fig. 14(a).

Figs. 11–14 provide useful design guidelines that are different from that provided using the FPT model. For example, one such guideline, according to [3], is that increasing I/stage is equally effective as increasing V_{swing} (and hence $V_{\text{ds(sat)}}$) in reducing cycle-to-cycle jitter. This is shown in Fig. 14(b), where a traditional FPT model is assumed. As an example, it is shown in the figure that for a jitter of 31 ps a I/stage of 4 μA with a V_{swing} of 1 V is required. When we decrease the V_{swing} (and hence $V_{\text{ds(sat)}}$) to 500 mV, the jitter is increased. To satisfy the same jitter requirement, we need to increase the I/stage to 8 μA , or by 2 times. Let us repeat the same exercise in Fig. 14(a). At the same jitter level of 31 ps, a I/stage of 20 μA with a V_{swing} of 1 V is required. When we decrease the V_{swing} to 500 mV, we need to compensate for the resulting increase in jitter, by increasing I/stage , to only 25 μA , or by 1.25 times. Therefore, in this example increasing I/stage is shown to be more effective in reducing jitter than increasing V_{swing} . This can also be shown to be true in general throughout other operating conditions and thus serves as a new useful design guideline.

Figs. 11–14 also quantify the noise level when LPT model is useful over FPT model in a practical application. For example, let us look at the IEEE standard 802.15.4 (low bit rate machine to machine communication, whose carrier is at 2.4 GHz and whose modulation scheme is similar to MSK), the total rms jitter is -15 dBc [19]. Assuming the frequency synthesizer is done using a DLL (which means α referenced in [3] is 1) then Δt_{cycle} is 74 ps. For a 4-stage ring oscillator, let us see for a Δt_{cycle} of 74 ps how much the result using a LPT model differs from that using a FPT model. Referring to Fig. 13, the LPT and FPT plots are seen to lead to a noticeable difference in I/stage : $1.5 \mu\text{A}/\text{stage}$ versus $5.5 \mu\text{A}/\text{stage}$, or 3.6 times. Hence, for this simplified example the oscillator is operating at a level where using the more detail LPT model is justified. As another example, Figs. 11–14 were applied to the design of ring oscillators in [10]

VI. CONCLUSION

This paper attempts to analyze one distinct aspect of the timing jitter of a ring oscillator when its delay cells are modeled as buffers and the noise sources are assumed to be thermal noise. This distinct aspect is the nature of the threshold crossing. The paper shows that the use of the LPT model for the threshold crossing gives us a more accurate description than the conventional FPT model when the noise/ramp ratio is not small. It also develops a link between the last passage and FPT model and indicates when the difference between the two models becomes significant. Simulation results on various design examples confirm the usefulness of this new model.

ACKNOWLEDGMENT

The author would like to thank Prof. R. Williams most deeply for her insightful discussions on the field of stochastic calculus, Prof. A. Heunis for introducing the author to this exciting field of stochastic calculus, Prof. D. Mcleish and Dr. N. Shah for all the help on the last passage time model, Prof. G. Freeman for answering all the author's questions on probability theory, C. Campbell for helping with Mathcad, and M. Sharifkhani for helping with simulations.

REFERENCES

- [1] A. Hajimiri and T. H. Lee, "A general theory of phase noise in electrical oscillators," *IEEE J. Solid-State Circuits*, vol. 33, p. 179, Feb. 1998.
- [2] B. Razavi, "A study of phase noise in CMOS oscillators," *IEEE J. Solid-State Circuits*, vol. 31, p. 331, Mar. 1996.

- [3] T. C. Weigandt, B. Kim, and P. R. Gray, "Analysis of timing jitter in CMOS ring oscillators," in *Proc. Int. Symp. Circuits Systems*, June 1994, pp. 4.27–4.30.
- [4] B. Kim, T. C. Weigandt, and P. R. Gray, "PLL/DLL system noise analysis for low jitter clock synthesizer design," in *Proc. Int. Symp. Circuits Systems*, June 1994, pp. 4.31–4.35.
- [5] B. Kim, "High-speed clock recovery in vlsi using hybrid analog/digital techniques," Ph.D. dissertation, Dept. of Elect. Eng. Comput. Sci., Univ. California, Berkeley, 1990.
- [6] T. Weigandt, "Low-phase-noise, low-timing-jitter design techniques for delay cell based VCOs and frequency synthesizers," Ph.D. dissertation, Dept. of Elect. Eng. Comp. Sci., Univ. California, Berkeley, 1998.
- [7] J. McNeill, "Jitter in ring oscillator," Ph.D. dissertation, Dept. of Elect. Eng. Comp. Sci., Boston Univ, Boston, MA, 1994.
- [8] B. Leung and D. Mcleish, "Investigation of phase noise of ring oscillators with time varying current and noise sources by time scaling thermal noise," *IEEE Trans. Circuits Syst. I*, to be published.
- [9] A. Hajimiri, S. Limotyrakis, and T. H. Lee, "Jitter and phase noise in ring oscillators," *IEEE J. Solid-State Circuits*, vol. 34, p. 790, June 1999.
- [10] Z. Shu, K. Lee, and B. Leung, "A 2.4-GHz. ring-oscillator-based CMOS frequency synthesizer with a fractional divider dual-PLL architecture," *IEEE J. Solid-State Circuits*, vol. 39, pp. 452–462, Mar. 2004.
- [11] B. Leung, *VLSI for Wireless Communication*. Englewood Cliffs, NJ: Prentice-Hall, 2002.
- [12] W. Yu and B. Leung, "Noise analysis for sampling mixers using stochastic differential equations," *IEEE Trans. Circuits Syst. II*, vol. 46, p. 699, June 1999.
- [13] S. Ross, *Probability Models*, 5th ed. New York: Academic, 1993.
- [14] G. Phillies, *Elementary Lectures in Statistical Mechanics*. New York: Springer-Verlag, 1999.
- [15] E. Lifshitz and L. Pitaevskii, *Statistical Physics*, 3rd ed. New York: Pergamon, 1980, pt. 1.
- [16] R. Durrett, *Stochastic Calculus, a Practical Introduction*. Boca Raton, FL: CRC, 1996.
- [17] I. Karatzas and S. Shreve, *Brownian Motion and Stochastic Calculus*. New York: Springer-Verlag, 1988.
- [18] D. Cox and H. Miller, *The Theory of Stochastic Processes*. London, U.K.: Chapman & Hall, 1977.
- [19] F. Martin, Private communication.



Bosco H. Leung (S'84–M'85–SM'92) received the B.Sc. degree from Rensselaer Polytechnic Institute, Troy, NY, in 1979, the M.Sc. degree from the California Institute of Technology, Pasadena, in 1980, and the Ph.D. degree from the University of California, Berkeley in 1987, all in electrical engineering.

From 1980 to 1983, he was an Analog Circuit Designer with Northern Telecom, Calgary, Canada. He joined the Department of Electrical and Computer Engineering, University of Waterloo, Waterloo, ON, Canada in 1988, where he is now a Professor.

His main research interest is in mixed analog–digital integrated circuits, in particular, wireless communication circuits and systems. He has published over 40 technical papers and has been granted four U.S. patents in this area. He is the author of the book *VLSI for Wireless Communication* (Englewood Cliffs, NJ: Prentice-Hall, 2002).

Dr. Leung was an Associate Editor for Communication Networks and RF Circuits for the IEEE TRANSACTIONS ON CIRCUITS AND SYSTEMS—II: ANALOG AND DIGITAL SIGNAL PROCESSING.